processes

MDPI

Article

A Model and the Characteristics of Gas Generation of the Longmaxi Shale in the Sichuan Basin

Xuewen Shi [1], Yi Li [1], Yuqiang Jiang [2,3,*], Ye Zhang [4], Wei Wu [1], Zhiping Zhang [4], Zhanlei Wang [2,3,*], Xingping Yin [2,3], Yonghong Fu [2,3] and Yifan Gu [2,3]

1 Shale Gas Research Institute, PetroChina Southwest Oil & Gasfield Company, Chengdu 610000, China; shixuewen@petrochina.com.cn (X.S.); liyi03@petrochina.com.cn (Y.L.); wwei06@petrochina.com.cn (W.W.)
2 School of Geoscience and Technology, Southwest Petroleum University, Chengdu 610500, China; yxp_swpu@163.com (X.Y.); fyh_swpu@163.com (Y.F.); xnsygyf@126.com (Y.G.)
3 Petrochina Key Laboratory of Unconventional Oil and Gas, Reservoir Evaluation Branch, Southwest Petroleum University, Chengdu 610500, China
4 National and Local Joint Engineering Research Center of Shale Gas Exploration and Development (Chongqing Institute of Geology and Mineral Resources), Chongqing 401120, China; zhangye_sg@vip.163.com (Y.Z.); zhangzhiping4211@163.com (Z.Z.)
* Correspondence: xnsyjyq3055@126.com (Y.J.); zlwang@swpu.edu.cn (Z.W.); Tel.: +86-13981828815 (Y.J.)

Abstract

Currently, the Longmaxi shale in the Sichuan Basin is the most successful stratum of shale gas production in China. However, because Longmaxi shale mostly has high over-maturity, a low-maturity sample cannot be obtained for gas generation thermal simulations, and as a result, a gas generation model has not yet been established for it. Therefore, models of other shales are usually used to calculate the amount of gas generated from Longmaxi shale, but they may produce inaccurate results. In this study, a Longmaxi shale sample with an equivalent vitrinite reflectance calculated from Raman spectroscopy (EqVR_o) of 1.26% was obtained from Well Yucan 1 in the Chengkou area, northeast Sichuan Province. This Longmaxi shale may have the lowest maturity in nature. Pyrolysis simulations based on gold tubes were performed on this sample, and the gas generation line was obtained. The amount of gas generated during the low-maturity stage was compensated by referring to gas generation data obtained from Lower Silurian black shale in western Lithuania. Thus, a gas generation model of the Longmaxi shale was built. The model showed that the gas generation process of Longmaxi shale could be divided into three stages: (1) First, there is the quick generation stage (EqVR_o 0.5–3.0%), where hydrocarbon gases were generated quickly and constantly, and the generation rate was steady. A maximum of 458 mL/g TOC was reached at a maturity of 3.0% EqVR_o. (2) Second, there is the stable stage (EqVR_o 3.0–3.25%), where the amount of generated gas reached a plateau of 453–458 mL/g TOC. (3) Third, there is the rapid descent stage (EqVR_o > 3.25%), where the amount of generated gas started to decrease, and it was 393 mL/g TOC at an EqVR_o of 3.34%. This model allows us to more accurately calculate the amount of gas generated from the Longmaxi shale in the Sichuan Basin.

Keywords: Sichuan Basin; Longmaxi shale; shale gas; gas generation model

check for updates

Academic Editor: Vijaya Raghavan

Received: 15 May 2025
Revised: 26 June 2025
Accepted: 11 July 2025
Published: 18 July 2025

Citation: Shi, X.; Li, Y.; Jiang, Y.; Zhang, Y.; Wu, W.; Zhang, Z.; Wang, Z.; Yin, X.; Fu, Y.; Gu, Y. A Model and the Characteristics of Gas Generation of the Longmaxi Shale in the Sichuan Basin. *Processes* **2025**, *13*, 2294. https://doi.org/10.3390/pr13072294

Copyright: © 2025 by the authors. Licensee MDPI, Basel, Switzerland. This article is an open access article distributed under the terms and conditions of the Creative Commons Attribution (CC BY) license (https://creativecommons.org/licenses/by/4.0/).

1. Introduction

The amount of gas generated is an important parameter in the resource evaluation of shale gas, and it is usually calculated from the gas generation model and the thermal

history of the studied shale. The general model of hydrocarbon generation suggests that oil is produced when the maturity of organic matter is in the vitrinite reflectance (R_o) range of 0.5–1.3%, and gas is the dominant product when R_o is higher than 1.3% [1]. In the high-maturity stage (R_o > 1.3%), the amount of gas produced from kerogen is limited, while gas produced from residual liquid hydrocarbons can account for ~70% of the gas generated in this stage [2]. Hill et al. [3] pointed out that the gas generated from residual liquid hydrocarbons was mostly in an R_o range of 1.3–2.0%. In commercial software for basin modeling (e. g., PetroMod, BasinMod, and BASIMS), different types of kinetic models of hydrocarbon generation can be used to calculate the amount of generated hydrocarbons by substituting the models into the thermal history of source rocks [4–6]. However, all of these models were established based on thermal simulations of typical source rocks with a low maturity, and these source rocks may differ from others in terms of hydrocarbon generation. Therefore, a specific kinetic model of the studied source rock can allow researchers to more precisely determine the amount of hydrocarbon generated.

In the thermal simulation of hydrocarbon generation, a source rock or kerogen is heated at different times and temperatures to generate hydrocarbons, and the amounts of hydrocarbons produced are recorded throughout the heating process [7–10]. In terms of samples, bulk source rocks and kerogen can be used. A small amount of kerogen can produce a lot of hydrocarbons; thus, the products can be quantified precisely. However, inorganic minerals, such as clays, may catalyze hydrocarbon generation [11]. Therefore, it is better to use bulk source rocks to investigate hydrocarbon generation models because the influence of inorganic minerals can be considered. Three types of systems can be used for the thermal simulation of hydrocarbon generation: open, closed, and semi-open systems. Among them, in open systems such as Rock-Eval, powered bulk shale samples (60–80 mesh) are heated, and the generated hydrocarbons are quantified using a flame ionization detector (FID). However, although this system is efficient and low-cost, it cannot be used to investigate the oil-cracking reaction [12]; thus, the gas generation capacity may be underestimated. In closed systems, such as gold tubes, the pressure can be considered, and the precise amounts of products can be determined; therefore, they are widely used to investigate hydrocarbon generation [10]. In gold tube systems, powered samples are heated under pressures similar to those of the subsurface, and all products, including oils and gases, are sealed in the tubes. Finally, the generated oils and gases are quantified by piercing the tubes using a needle in the high vacuum line. In semi-open systems, the in situ pyrolysis of organic matter in source rocks can be simulated [13], and both bulk samples and powered samples can be used. Hydrostatic and lithostatic pressures can be considered at the same time. Therefore, semi-open systema are considered as the best choice for simulating subsurface conditions; however, they are time-consuming and expensive. The kinetic parameters, including activation energy and frequency factor, are usually obtained according to the Arrhenius equation based on experimental results with two or more heating rates.

In this study, to precisely determine the amount of gas generated and consider the pressure, thermal simulations were performed on bulk shale using gold tubes. Usually, the pressure is kept stable in thermal simulations using gold tubes [14]; however, the pressure actually increases with an increasing burial depth. Therefore, to more accurately simulate the geological situation, different hydrostatic pressures were set according to the heating temperature. Although many previous studies found that water played an important role in hydrocarbon generation reactions [7,15], the kinetic parameters from hydrous and anhydrous pyrolysis experiments were similar [16,17], implying that water actually played a small role [18]. The previous experiments showed that the water generation ended when the vitrinite reflectance reached 1.2% [19]. The water content in shales decreased

significantly when the equivalent vitrinite reflectance was greater than 1.5% [20]. Therefore, we speculated that water played a small role in gas generation at the highly mature stage due to its low content and conducted anhydrous thermal simulations.

Longmaxi shale is currently the most successful stratum for shale gas exploration and production in China. To date, three national marine shale gas demonstration areas have been established, namely Jiaoshiba, Weiyuan-Changning, and Zhaotong, and many shale gas fields have been discovered [21]. However, there is no specific gas generation model for Longmaxi shale because its equivalent vitrinite reflectance values are mainly in the range of 2.0–4.0%, which cannot be used to conduct thermal simulations of gas generation [22]. In previous studies, the amount of gas generated from Longmaxi shale was calculated using gas generation models of other shales, such as the Xiamaling and Baltic shales [23]. It should be noted that the chemical composition of the organic matter in these shales and the Longmaxi shale may differ; thus, the calculated results are probably unreliable. Therefore, to establish a specific gas generation model for Longmaxi shale, seeking shale samples with a relatively low maturity from the Longmaxi Formation is crucial.

The Longmaxi shale from Well Yucan 1 has a relatively low maturity (~1.3%R_o) [24]; thus, a gas generation model for Longmaxi shale could be established by conducting thermal simulations on samples from this well. Consequently, in this study, we obtained a Longmaxi shale sample from Well Yucan 1 and conducted thermal simulations on it using gold tubes. The gas generation line was measured, and then the amount of gas generated in the vitrinite reflectance range of 0.5–1.3% was determined according to data obtained from a lower Silurian shale sample in the western region of Lithuania. A gas generation model of Longmaxi shale was finally established, and this model can be used to precisely calculate the amount of gas generated from Longmaxi shale.

2. Sample and Methods

2.1. Sample

Longmaxi shale was deposited in the period of marine transgression during the Early Silurian [25]. The sedimentary depocenters are in the southern Sichuan Basin (Figure 1). Its thickness varies from 20 m to 100 m in the southern and eastern Sichuan Basin (Figure 1). The dominant lithologies of this shale are siliceous and carbonaceous shales. The Longmaxi Formation is divided into two sections according to its lithological composition. Section 1 is in the lower part and is mainly composed of organics-rich black carbonaceous shale, siliceous shale, and dark gray arenaceous shale; graptolites are abundant [22]. Section 2 is in the upper part and is mainly composed of grayish-yellowish green shale and arenaceous shale interbedded with siltstone and marlstone. Section 1 is further divided into two layers. Layer 1 ($Long_1^1$) is in the lower part of Section 1 and is predominantly composed of black shale, and it is divided into four sub-layers of 1–4 from the bottom to the top. Among them, sub-layer 1 is composed of organics-rich black shale and is the main gas-producing layer of Longmaxi shale. Well Yucan 1 is located in the northeast of the Sichuan Basin (Figure 1), and it drills the Upper Ordovician and Lower Silurian strata (Figure 2). The sample used in this study was obtained from sub-layer 1 of layer 1 in Section 1 of the Longmaxi Formation at 1202.85 m–1202.92 m of Well Yucan 1, Chengkou, Chongqing (Figures 1–3).

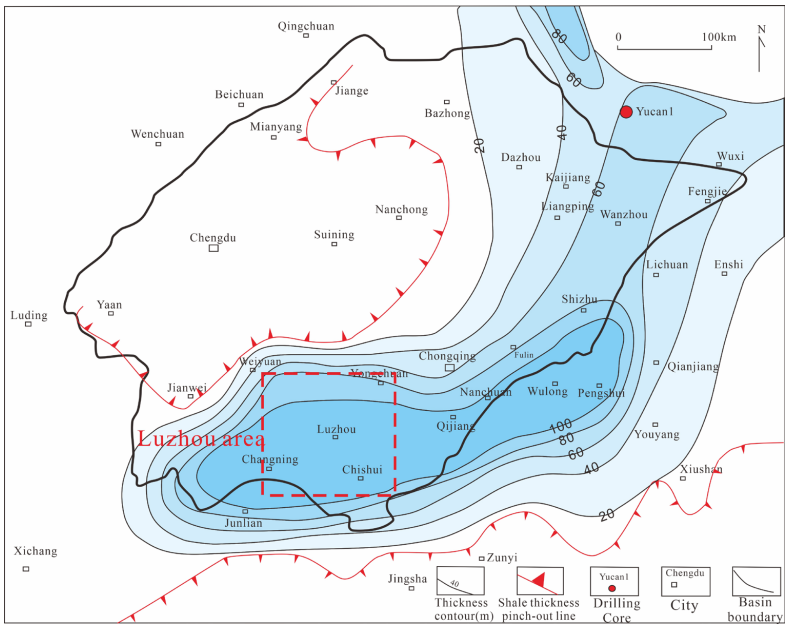

Figure 1. Locations of Well Yucan 1 and the Luzhou area (modified from Wang et al. [16]).

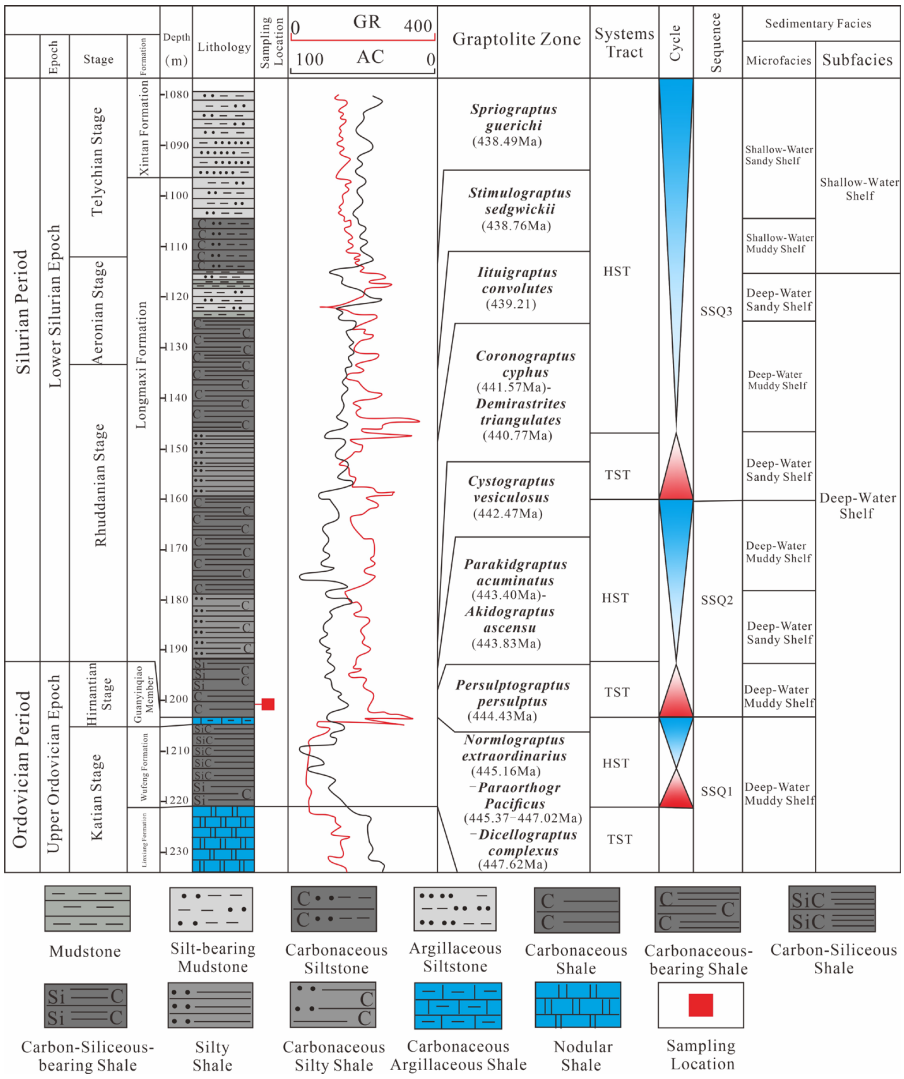

Figure 2. Stratigraphic framework and sampling location of Well Yucan 1 (modified from Zhang et al. [26]). HST: highstand system tract; TST: transgressive system tract; SSQ1: second-order

sequence 1; SSQ2: second-order sequence 2; SSQ3: second-order sequence 3; GR: the well log parameter of natural gamma rays, API; AC: the well log parameter of acoustics, μs/ft.



Figure 3. Sample obtained from Longmaxi Formation at 1202.85 m–1202.92 m of Well Yucan 1.

2.2. Methods

Each sample was crushed into 100 mesh powders with a pestle and mortar. Then, pyrolysis parameters and TOC content in the powdered samples were measured using a Rock-Eval 6 instrument manufactured by Vinci Technologies, Paris, France, and a CS-230 Elemental Analyzer made by LECO, Michigan, USA, according to the methods described by Han et al. [27]. Raman spectra were measured using an inVia Qontor LabRAM spectrometer produced by Renishaw, Gloucestershire, Britain. The equivalent vitrinite reflectance value was calculated based on the equation established by Liu et al. [28]. A piece of the studied shale sample was prepared according to ISO 7404-2 [29] for solid bitumen reflectance measurement. Solid bitumen reflectance was measured using a ZEISS AX10 microscope with an integrated TIDAS CCD UV/NIR microscope photometer produced by J&M in an oil immersion objective (50× magnification) according to ASTM D7708-14 [30].

Thermal simulations were performed on the chosen shale sample using gold tubes without water. The instrument and experimental steps were described by Gai et al. [14]. The powdered samples (200–500 mg) were filled into gold tubes, which were welded at one end, and then all tubes were flooded for 25 min using argon to remove the air in them. The other end of each tube was welded under the protection of argon and placed into a stainless-steel vessel. The heating temperatures ranged from 420 °C to 610 °C (Table 1), and the confined pressures varied from 15 MPa to 60 MPa (Table 1); two heating rates, 2 °C/h and 20 °C/h, were used, respectively. The EasyR_o values (Table 1) were calculated according to the method described by Sweeny and Burnham [31]. During the simulations, the accuracy of the temperature was less than ±0.5 °C, and the accuracy of the pressure was ±1 MPa. When each heating experiment was finished, the stainless-steel vessel was removed from the oven and quickly cooled by quenching it in water at room temperature.

Table 1. Experimental scheme of the thermal simulations using gold tubes.

Heating Rate (°C/h)	Confined Pressure (MPa)	Final Temperature (°C)	EasyR_o (%)	Time at Final Temperature (h)
20	15	460	1.50	0
	20	490	2.00	0
	25	520	2.50	0
	30	550	3.02	0
	35	575	3.48	0
	40	609	4.01	0
	45	610	4.53	12

Table 1. *Cont.*

Heating Rate (°C/h)	Confined Pressure (MPa)	Final Temperature (°C)	EasyR_o (%)	Time at Final Temperature (h)
20	50	610	4.68	24
	55	610	4.69	48
2	15	420	1.52	0
	20	450	1.98	0
	25	480	2.30	0
	30	500	2.91	0
	35	530	3.49	0
	35	560	3.98	0
	40	600	4.53	0
	50	600	4.63	12
	60	600	4.68	48

The cooled tubes were pierced using a needle in the high vacuum line at room temperature, and the gaseous products were collected. The generated gases were then pumped into a calibrated volume to measure their volume. The gases were finally injected into a 7890A gas chromatograph, manufactured by Agilent Technologies, Inc., California, USA, for a composition analysis according to the method described by Gai et al. [14]. The stable carbon isotopic compositions of the produced gas were analyzed using a VG Isochrom II isotope ratio mass spectrometer according to the methods described by Wang et al. [32]. The solid residuals from each thermal simulation were used to measure Raman spectra using the method given above, and the equivalent vitrinite reflectance values were also calculated using the equation established by Liu et al. [28].

3. Results

3.1. Geochemical and Mineralogical Information of the Starting Sample

The geochemical parameters of the starting sample are shown in Table 2. The TOC content is 4.17%; The T_{max} is 472 °C; and S_1, S_2, and HI are 0.36 mg/g, 2.71 mg/g, and 64.99 mg/g TOC, respectively. The equivalent vitrinite reflectance calculated from Raman spectra data according to the equation given by Liu et al. [28] is 1.26%, and that calculated from the reflectance of solid bitumen is 1.49% (Table 2 and Figure 4), suggesting that the starting sample has a relatively high maturity.

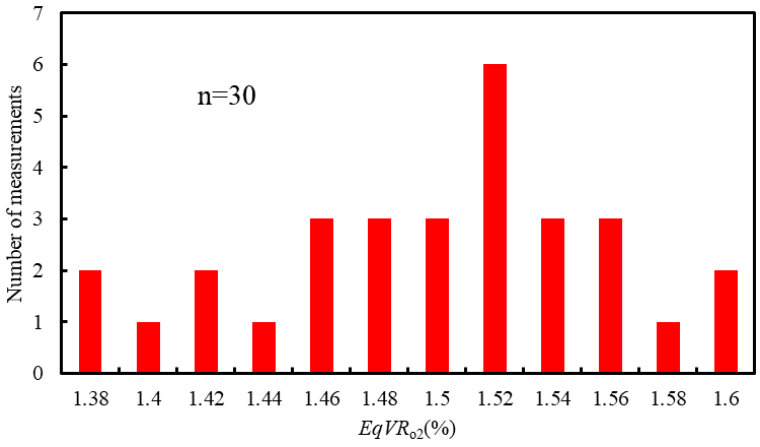

Figure 4. The equivalent vitrinite reflectance (EqVR_{o2}) histogram of the starting sample (EqVR_{o2} represents the equivalent vitrinite reflectance calculated from the reflectance of solid bitumen according to the equation established by Jacob [33]).

Table 2. Geochemical parameters of the starting sample.

TOC (%)	T_{max} (°C)	S_1 (mg/g)	S_2 (mg/g)	S_3 (mg/g)	HI (mg/g TOC)	OI (mg/g TOC)	* EqVR_{o1} (%)	** EqVR_{o2} (%)
4.17	472	0.36	2.71	0.32	64.99	7.67	1.26	1.49

* EqVR_{o1} represents the equivalent vitrinite reflectance calculated from Raman spectra data according to the equation given by Liu et al. [28]. ** EqVR_{o2} represents the equivalent vitrinite reflectance calculated from the reflectance of solid bitumen according to the equation established by Jacob [33].

The mineralogical composition of the starting sample is listed in Table 3. The sample is mostly composed of quartz, with a content of 37.3%. The mixed layer of illite and smectite accounts for 31.1%, followed by feldspar (11.4%), pyrite (8.3%), and dolomite (6.8%).

Table 3. Mineral composition of the starting sample.

Quartz (%)	Feldspar (%)	Dolomite (%)	Pyrite (%)	Kaolinite (%)	Chlorite (%)	Illite (%)	** I/S (%)	*** C/S (%)
37.3	11.4	6.8	8.3	0.35	1.33	2.12	31.1	1.3

** I/S represents the mixed layer of illite and smectite. *** C/S represents the mixed layer of chlorite and smectite.

3.2. Gas Yield

The amounts of gaseous hydrocarbons (including methane, ethane, propane, butane, and pentane) showed a variation of three stages (Figure 5). In the thermal simulations with a heating rate of 20 °C/h, the amounts first increased from 38.82 mL/g TOC to 407.13 mL/g TOC when the EqVR_o values were between 1.3% and 3.07% (Figure 5 and Table 4), and then they started to decrease. At a heating rate of 2 °C/h, the generated hydrocarbons first increased from 40.5 mL/g TOC to 351.11 mL/g TOC in the EqVR_o range of 1.47–3%, and then they remained stable in the EqVR_o range of 3–3.25% (Figure 5) and finally decreased when the EqVR_o exceeded 3.25% (Figure 5). The difference between the two heating rates in terms of the variations in the generated hydrocarbons may be attributed to the fact that the gaseous products had a longer time to achieve balance in the experiments with a slower heating rate.

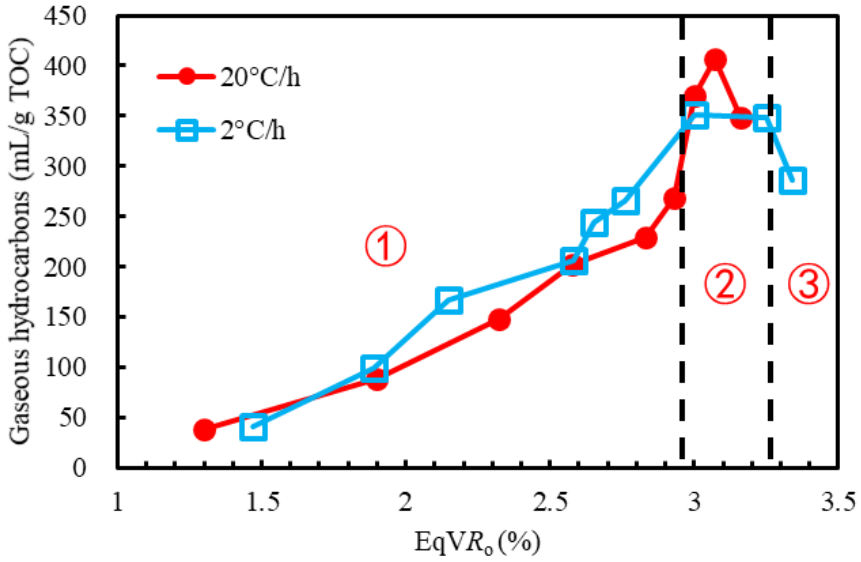

Figure 5. Total gaseous hydrocarbon generation lines obtained from thermal simulations using gold tubes. ① stage 1 (1.3–3.0%, EqVR_o), generated gases increased quickly; ② stage 2 (3.0–3.25%, EqVR_o), generated gases were stable; ③ stage 3 (EqVR_o > 3.25%), generated gases decreased.

Table 4. Generated gaseous hydrocarbons obtained from thermal simulations using gold tubes.

Heating Rate (°C/h)	Final Temperature (°C)	EqVR_o (%)	Generated Gas (mL/g TOC)						
			Methane (C_1)	Ethane (C_2)	Propane (C_3)	Butane (C_4)	Pentane (C_5)	C_{2-5}	C_{1-5}
20	460	1.3	28.45	7.70	2.26	0.31	0.02	10.37	38.82
	490	1.9	73.89	12.06	2.03	0.15	0.00	14.27	88.16
	520	2.32	136.52	10.88	0.61	0.01	0.00	11.51	148.03
	550	2.58	196.01	5.60	0.05	0.00	0.00	5.66	201.66
	575	2.83	226.87	2.26	0.01	0.00	0.00	2.27	229.14
	609	2.93	267.09	1.43	0.00	0.00	0.00	1.43	268.52
	610	3	370.04	0.42	0.00	0.00	0.00	0.42	370.46
	610	3.07	407.13	0.00	0.00	0.00	0.00	0.00	407.13
	610	3.16	348.47	0.33	0.00	0.00	0.00	0.33	348.80
2	420	1.47	29.85	8.06	2.24	0.31	0.03	10.65	40.50
	450	1.89	84.37	12.85	1.85	0.14	0.00	14.85	99.22
	480	2.15	157.21	9.56	0.30	0.01	0.00	9.87	167.07
	500	2.58	201.13	4.79	0.05	0.00	0.00	4.84	205.97
	530	2.65	242.42	1.56	0.02	0.00	0.00	1.58	244.00
	560	2.76	265.02	0.92	0.01	0.00	0.00	0.93	265.95
	600	3	350.77	0.34	0.00	0.00	0.00	0.34	351.11
	600	3.25	347.71	0.34	0.00	0.00	0.00	0.34	348.05
	600	3.34	286.05	0.29	0.00	0.00	0.00	0.29	286.34

3.3. Gas Compositions

The variation in the generated methane content is similar to that in the gaseous hydrocarbons, and it can also be divided into three stages (Figure 6a, Table 4). The heavier gaseous hydrocarbons (ethane (C_2), propane (C_3), butane (C_4), and pentane (C_5)) have three stages of change (Figure 6b and Table 3), including a quick increase (EqVR_o 1.5–2.0%), a rapid decrease (EqVR_o 2.0–2.6%), and a slow decrease (EqVR_o > 2.6%). The line of the heating rate of 2 °C/h is a little lower than that of 20 °C/h, which may be related to the reason given above.

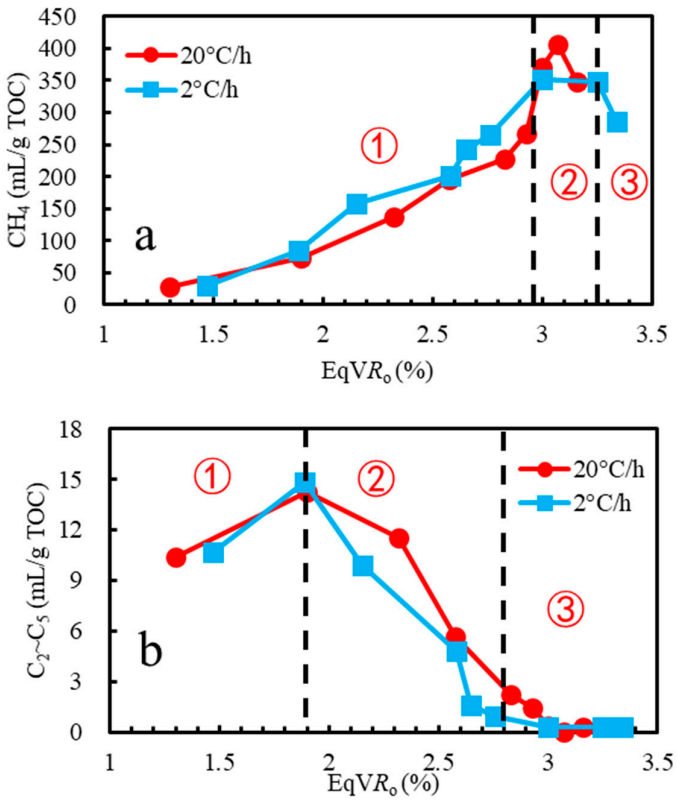

Figure 6. Gas generation lines obtained from thermal simulations using gold tubes. (**a**) The amount of methane (CH_4) varied with the increasing EqVR_o, ① stage 1 (1.3–3.0%, EqVR_o), generated methane

increased quickly; ② stage 2 (3.0–3.25%, EqVR_o), generated methane was stable; ③ stage 3 (EqVR_o > 3.25%), generated methane decreased; (**b**) the amount of heavier gaseous hydrocarbons (C_2–C_5) varied with the increasing EqVR_o, ① stage 1 (1.5–2.0%, EqVR_o), generated C_2–C_5 increased quickly; ② stage 2 (2.0–2.6%, EqVR_o), generated C_2–C_5 decreased quickly; ③ stage 3 (EqVR_o > 2.6%), generated C_2–C_5 decreased slowly.

3.4. Carbon Isotopic Composition

During the thermal simulations, the stable carbon isotope values of ethane ($\delta^{13}C_2H_6$) were heavier than those of methane ($\delta^{13}CH_4$), and the corresponding values of propane ($\delta^{13}C_3H_8$) were larger than those of $\delta^{13}C_2H_6$, all of which increased in this process (Figure 7 and Table 5). It should be noted that the ($\delta^{13}CH_4$) values for the heating rate of 20 °C/h decreased at the EqVR_o of 3%, and there was also a small decrease in the line of 2 °C/h at the EqVR_o of 3.34%, which may be related to the decrease in the amounts of methane (Figure 6a), as the bond between ^{12}C and ^{12}C is more easily ruptured than that between two ^{13}C atoms.

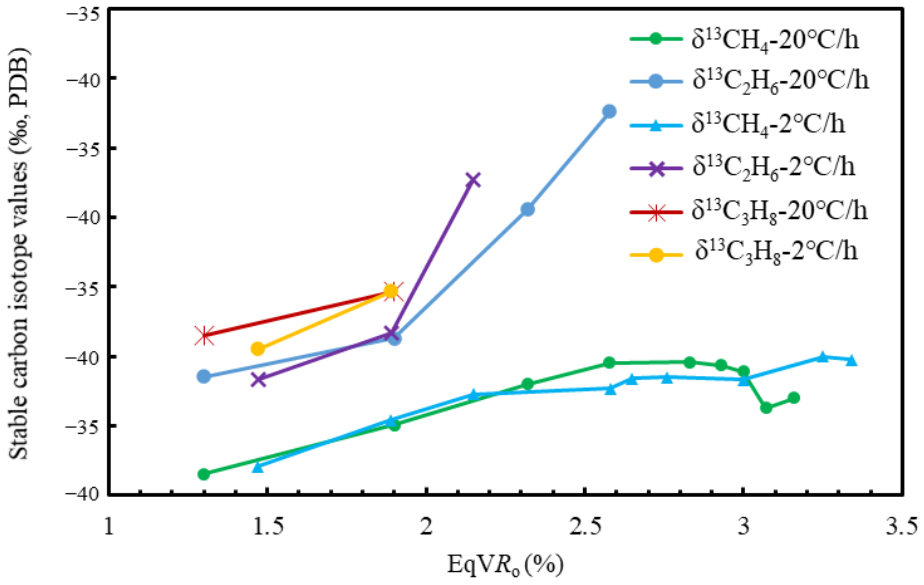

Figure 7. Stable carbon isotope values of methane and ethane obtained from thermal simulations using gold tubes.

Table 5. Stable carbon isotope values of the generated gaseous hydrocarbons obtained from thermal simulations using gold tubes.

Heating Rate (°C/h)	Final Temperature (°C)	EqVR_o (%)	Stable Carbon Isotope Values (‰, PDB)		
			Methane ($\delta^{13}C_1$)	Ethane ($\delta^{13}C_2$)	Propane ($\delta^{13}C_3$)
20	460	1.3	−38.43	−31.43	−28.45
	490	1.9	−34.93	−28.7	−25.37
	520	2.32	−32.01	−19.43	
	550	2.58	−30.46	−12.37	
	575	2.83	−30.43		
	609	2.93	−30.63		
	610	3	−31.1		
	610	3.07	−33.69		
	610	3.16	−32.97		
2	420	1.47	−37.91	−31.68	−29.5
	450	1.89	−34.57	−28.29	−25.36
	480	2.15	−32.7	−17.3	
	500	2.58	−32.32		
	530	2.65	−31.59		
	560	2.76	−31.48		

Table 5. *Cont.*

Heating Rate (°C/h)	Final Temperature (°C)	EqVR_o (%)	Stable Carbon Isotope Values (‰, PDB)		
			Methane ($\delta^{13}C_1$)	Ethane ($\delta^{13}C_2$)	Propane ($\delta^{13}C_3$)
2	600	3	−31.68		
	600	3.25	−30		
	600	3.34	−30.21		

4. Discussion

4.1. Origin of Gas

Most of the gases from the shale gas reservoirs (Weiyuan, Changning, and Jiaoshiba shale gas fields) in the Longmaxi shale have a mixed-origin character with negative carbon isotopes, according to the plot established by Dai [34] (Figure 8). However, the gas samples from the thermal simulations in this study were in the areas of I, II, and IV (Figure 8), indicating their complex origins. In this study, because the starting sample was one marine shale, it mainly contained type II organic matter; additionally, as the gases produced by type II organic matter cannot be coal-derived gases, the gases obtained from the simulations should be oil-type ones. The plot of Ln (C_1/C_2)-Ln (C_2/C_3) showed that the gases from natural shale gas fields were generated by oil-cracking (Figure 9), while most of the gases obtained from the thermal simulations in this study were produced by kerogen-cracking, which was caused by the relatively high maturity of the starting sample, in which the amount of residual liquid hydrocarbons was limited (Table 3).

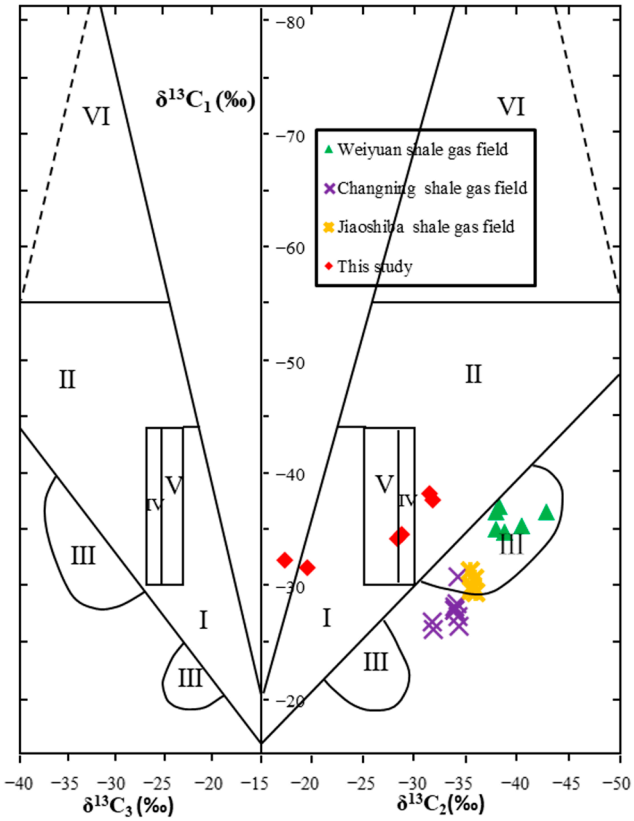

Figure 8. The determination of gas origin of shale gas from the Longmaxi Formation (chart according to Dai [34]) (I. Coal-derived gas, II. Oil-type gas, III. Mixed gas with negative carbon isotopes, IV. Coal-derived gas or oil-type gas, V. Coal-derived gas, oil-type gas, or mixed gas, and VI. Biogenic gas. The data of Weiyuan, Changning, and Jiaoshiba shale gas fields were after Dai et al. [35]).

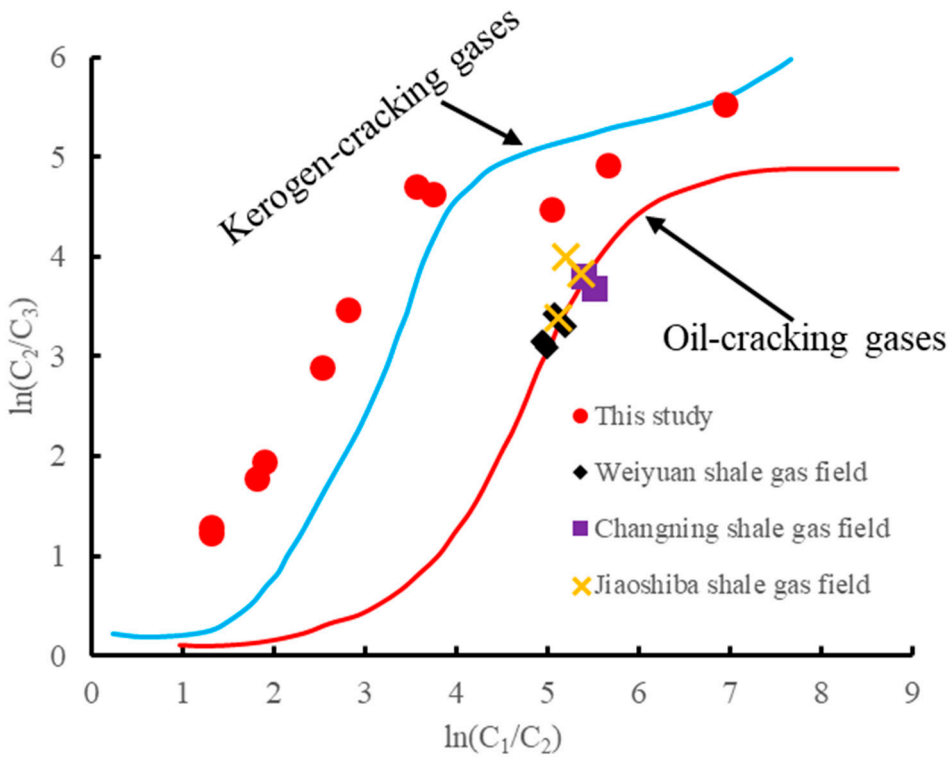

Figure 9. Identification of kerogen-cracking gas and oil-cracking gas using plot of Ln (C_1/C_2)-Ln (C_2/C_3) (chart according to Li et al. [36]). The data of Weiyuan, Changning, and Jiaoshiba shale gas fields were after Dai et al. [35]).

4.2. Gas Generation Model

As the starting sample used in the thermal simulations had an equivalent reflectance (EqVR_o) of 1.26% (Table 3), the gas generated in the lower mature stage could not be quantified from the thermal simulation results. Therefore, the amount of gas produced when the EqVR_o value was lower than 1.26% needed to be compensated. Ma et al. [37] conducted a set of thermal simulations using a lowly mature shale sample (0.56%EqVR_o) from the Lower Silurian in the western part of Lithuania to obtain its gas generation line (Figure 10). The Lower Silurian shale that they used is considered to be the most similar to the Longmaxi shale because they have a similar sedimentary time and environment [23]. The paleogeographic location of the Lithuania shale relative to southern China is the mid-Silurian; it contains alga type II kerogen, and the macerals include graptolites, algae, and plankton bacteria [38]. In general, it is similar to the Longmaxi shale in terms of lithology, kerogen type, depositional age, and sedimentary environment. Consequently, we took the amount of gas generated from the Lithuania sample when the EasyR_o was lower than 1.26% to compensate the gas generated in the same mature range for the studied sample, and a gas generation model of the Longmaxi shale was established (Figure 11).

It should be noted that the EqVR_o values were generally lower than EasyR_o ones (Tables 1 and 4); because the EasyR_o model was established based on the vitrinite reflectance data from coal samples [31], we believe that EqVR_o can give more credible mature information. Therefore, the EqVR_o values were used in this study. The gas generation process of the Longmaxi shale can be divided into three stages (Figure 11): (1) At EqVR_o 0.5–3.0%, the amount of gas generated increased rapidly, the gas generation speed was stable, and a total of 458 mL/g TOC gases was produced at the end of this stage. Both kerogen-cracking gases and liquid hydrocarbon-cracking gases contributed to the gas generation in this stage. (2) At the EqVR_o range of 3.0–3.25%, the amount of gas generated had no obvious changes, indicating that gas generation potentials were depleted.

(3) At EqVR_o > 3.25%, the amount of gas generated decreased quickly, and it dropped to 393 mL/g TOC at the EqVR_o of 3.3% (Figure 11), which was caused by the onset of methane decomposition [39,40].

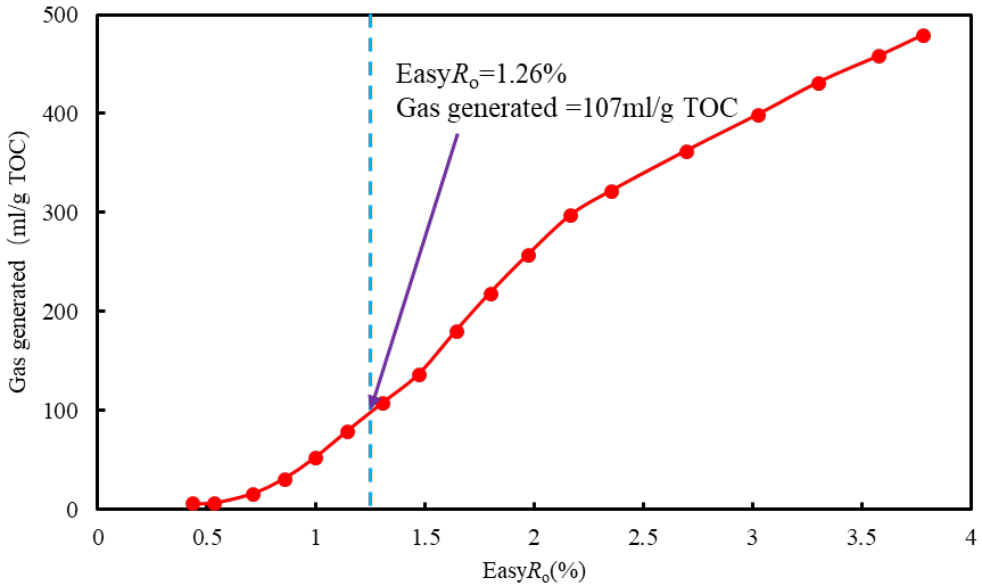

Figure 10. Gas generation of the Lower Silurian black shale from eastern Lithuania (based on the study by Ma et al. [37]).

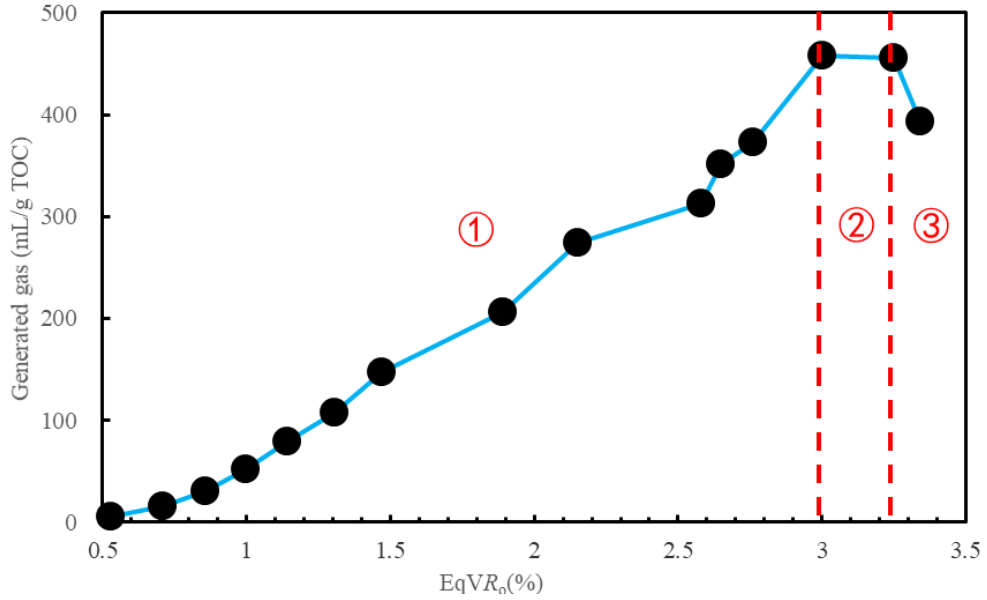

Figure 11. Gas generation model of the Longmaxi shale. ① stage 1 (0.5–3.0%, EqVR_o), generated gases increased quickly; ② stage 2 (3.0–3.25%, EqVR_o), generated gases were stable; ③ stage 3 (EqVR_o > 3.25%), generated gases decreased quickly.

Our results show that the gas generation of Longmaxi shale ended at the EqVR_o of 3.25% (Figure 11), which is close to the maturity limit of 3.0%R_o published by Horsfield et al. [23], who proposed this limit after comparing the chemical structures of kerogen and the results of thermal simulations of many marine shales. However, the maximum amount of gas generated from Longmaxi shale was 458 mL/g TOC, which is higher than the 335 mL/g TOC of Xiamaling shale [41] but lower than the 480 mL/g TOC of the Lower Silurian shale in the Western part of Lithuania [37]. Therefore, the gas generation model

established in this study allows us to precisely determine the amount of gas generated from the Longmaxi shale in the Sichuan Basin.

4.3. Application

To test the gas generation model established in this study, we applied it to sub-layer 1 of layer 1 of Section 1 of the Longmaxi ($Long_1^1$) shale in the Luzhou area of the southern Sichuan Basin (Figure 1). The shale thickness of sub-layer 1 of $Long_1^1$ was in the range of 1–2.5 m, and the shale thickness in the Nanxi–Changning area was relatively large (Figure 12). The contour map of the TOC content was obtained using the date from the wells shown in Figure 13. The TOC contents of the Longmaxi shales in the Luzhou area were generally greater than 4%, with most of them having values between 5% and 6%, and the shales in the Luxian–Nanxi area had relatively high TOC contents (Figure 13). The contour map of the equivalent vitrinite reflectance was drawn according to the reflectance values from the wells shown in Figure 14, and the relationship between EqVR_o and depth was also referenced. The equivalent vitrinite reflectance values of the shales in the Luzhou area were mostly in the range of 3.3–3.5%, the shales in the middle of the Luzhou area had higher maturities, and the equivalent vitrinite reflectance values decreased around the middle area (Figure 14). The Longmaxi shale in the Luzhou area was deposited in deep water shelf environment, and the organic matter and mineral compositions showed no obvious changes. Therefore, we regarded the Longmaxi shale in the Luzhou area as a whole to estimate its amount of gas generated.

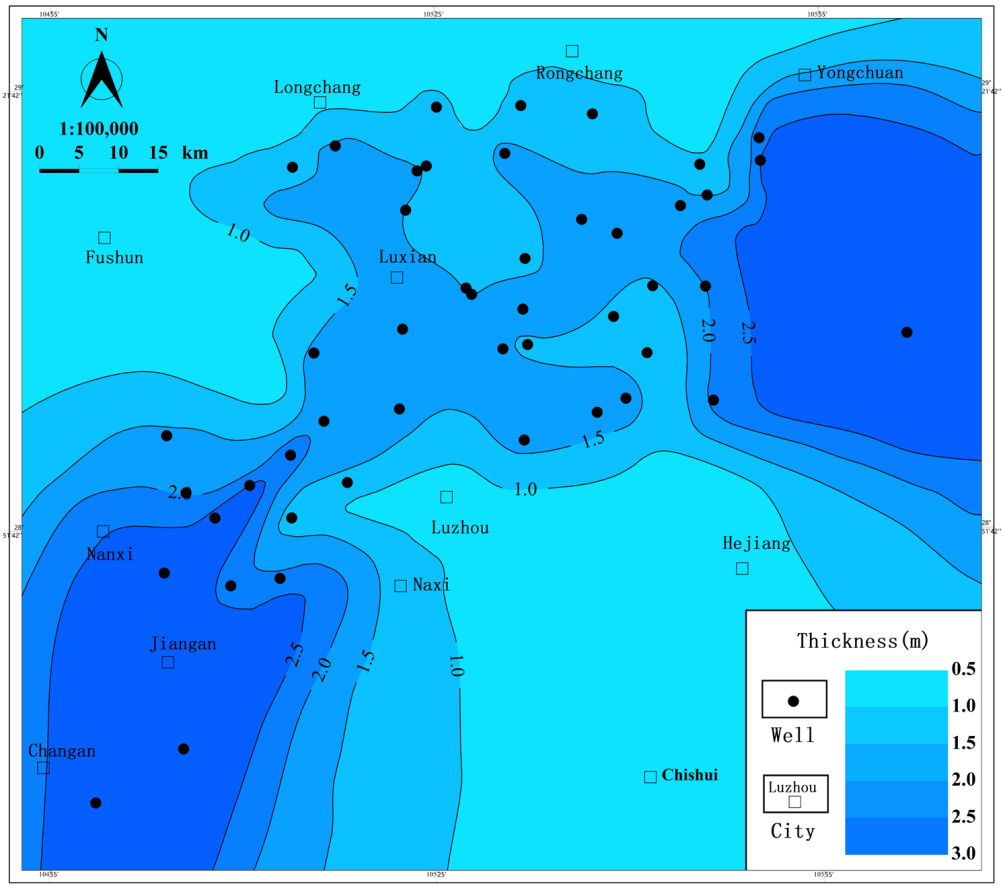

Figure 12. Contour map of shale thickness in sub-layer 1 of $Long_1^1$ in the Luzhou area.

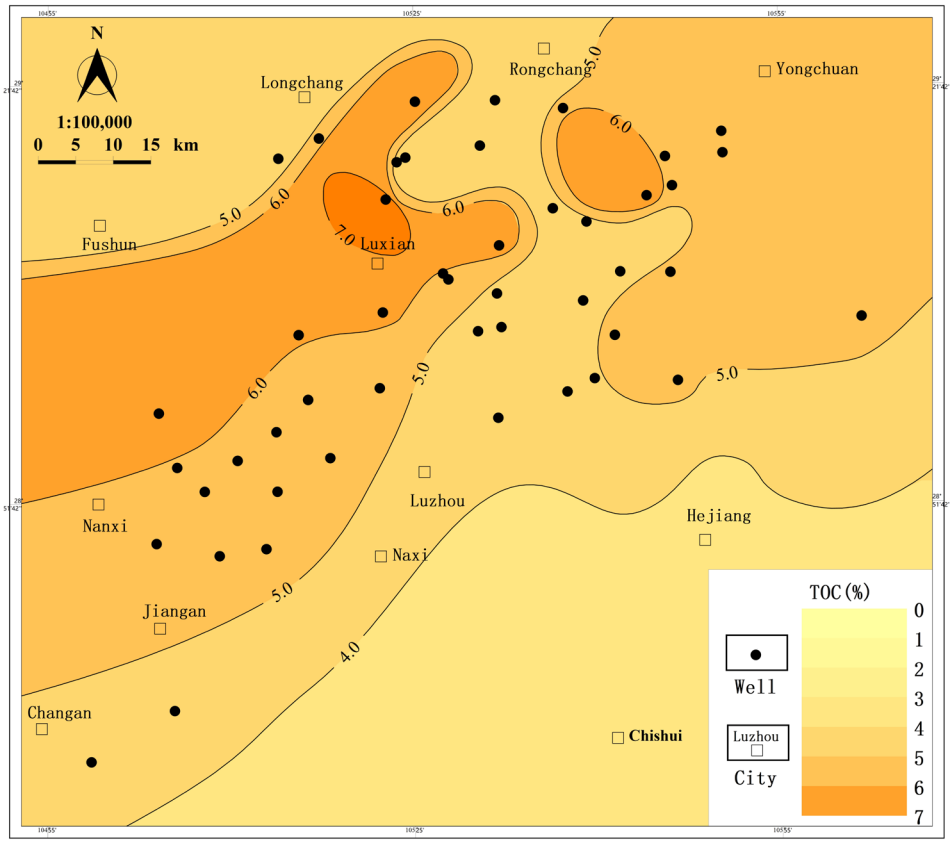

Figure 13. Contour map of the TOC content in sub-layer 1 of $Long_1^1$ in the Luzhou area.

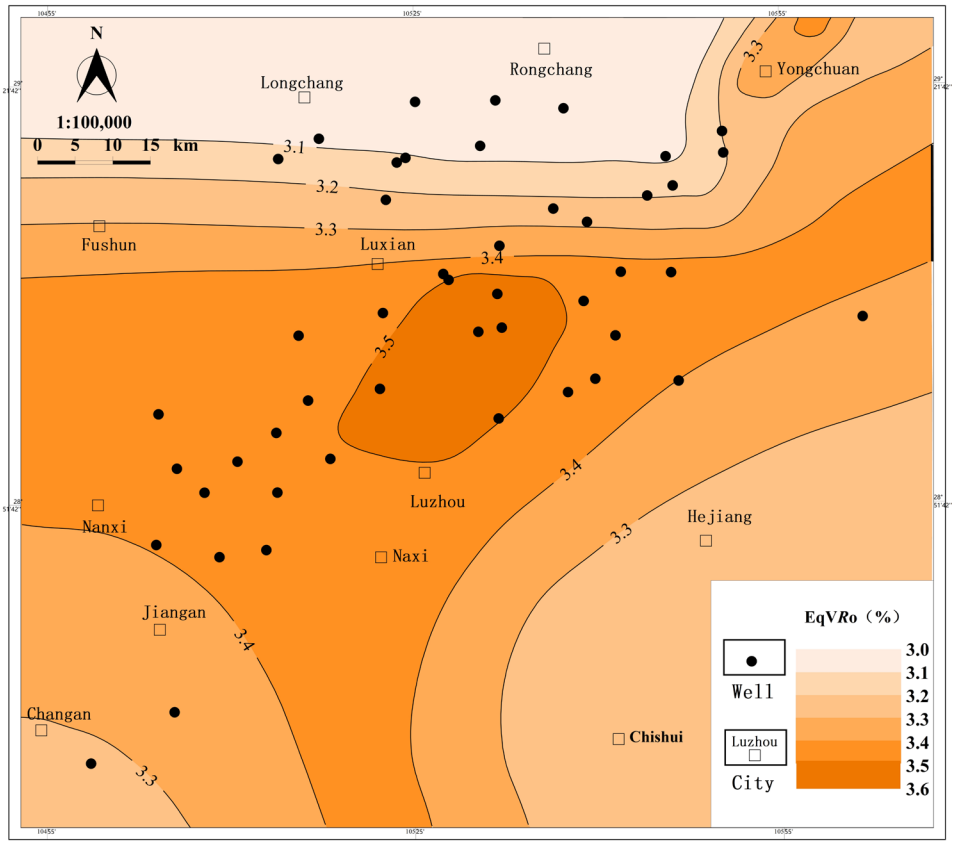

Figure 14. Contour map of $EqVR_o$ in sub-layer 1 of $Long_1^1$ in the Luzhou area.

Based on the contour maps above (Figures 12–14) and the gas generation model (Figure 11), we used the equation below to calculate the amount of gas generated from sub-layer 1 of $Long_1^1$ in the Luzhou area, as well as the gas generation intensity.

$$E = (H \times D \times C \times Q)/100$$

where E represents the gas generation intensity (10^8 m^3/km^2); H is the shale thickness (m); D is the shale density (t/m^3), with 2.548 t/m^3 used in this calculation; C is the shale organic matter content, which was calculated by dividing the TOC by 100 (TOC/100); and Q is the gas yield (mL/g TOC).

The results show that the gas generation intensity in sub-layer 1 of $Long_1^1$ in the Luzhou area ranged from 0.4×10^8 m^3/km^2 to 1.6×10^8 m^3/km^2, and the shales in the Nanxi–Changning area had relatively high gas generation intensities (Figure 15). The total amount of gas generated in sub-layer 1 of $Long_1^1$ in the Luzhou area was about 1.0×10^{12} m^3. Previous researchers used the gas generation model of a Devonian shale sample from the Luquan area of Yunnan Province, southwestern China, to calculate the amount of gas generation from the Longmaxi shale [42]. We also computed the gas generation of sub-layer 1 of $Long_1^1$ in the Luzhou area, and the results show that the gas generation intensities were between 0.2×10^8 m^3/km^2 and 0.6×10^8 m^3/km^2 (Figure 16). The total amount of gas generated was 0.4×10^{12} m^3, which is much lower than the value obtained using the model proposed in this study, suggesting that the gas generation capacity of shales was seriously underestimated.

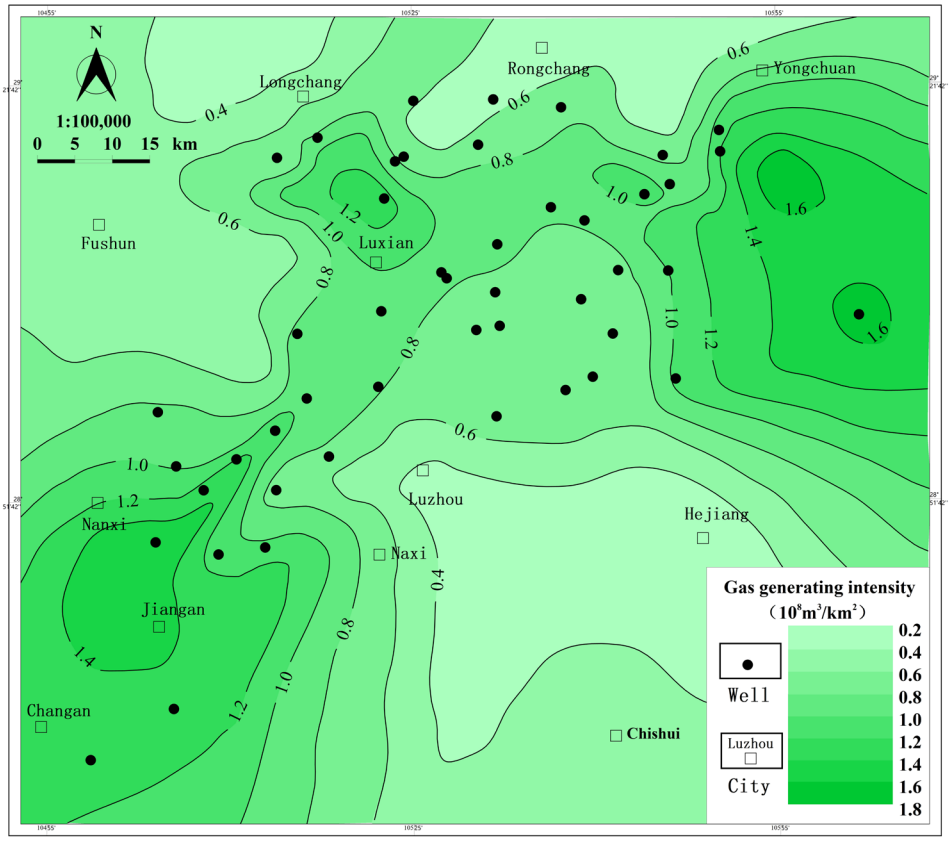

Figure 15. Contour map of gas generation intensity from sub-layer 1 of $Long_1^1$ in the Luzhou area (calculated according to the gas generation model proposed in this study).

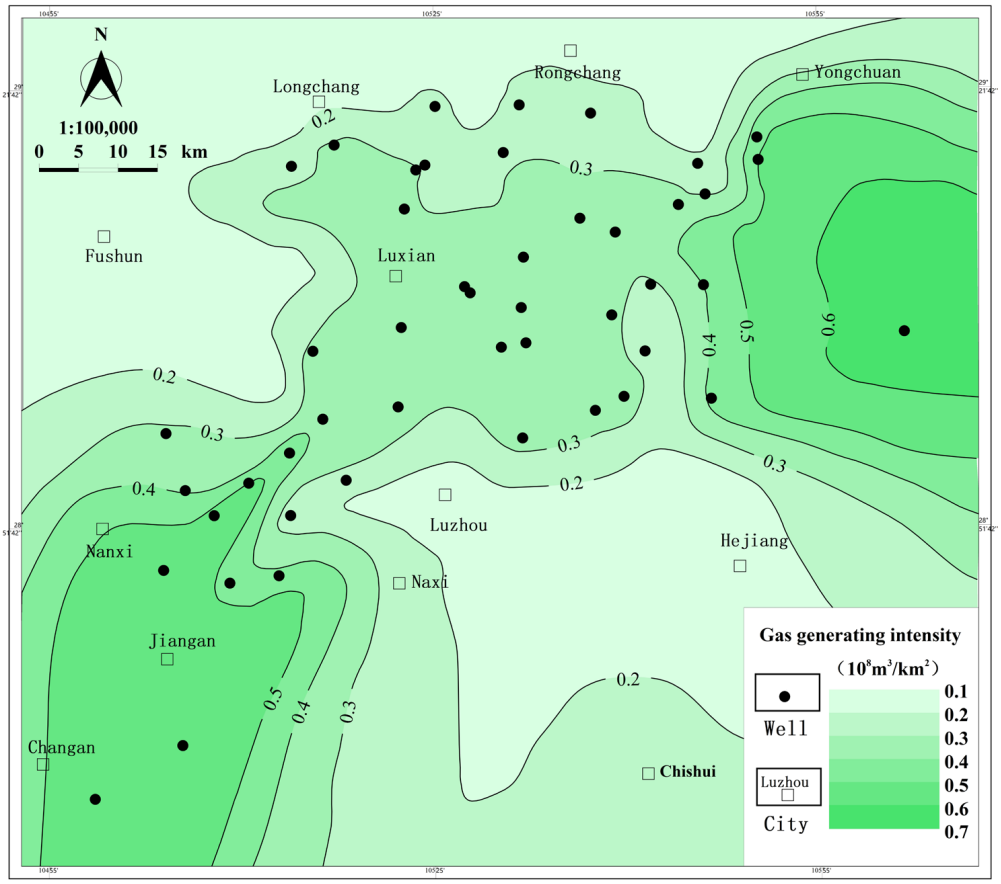

Figure 16. Contour map of gas generation intensity from sub-layer 1 of $Long_1^1$ in the Luzhou area (calculated according to the gas generation model in the study by Guo et al. [42]).

The contour map of gas content was drawn according to the gas contents from the wells shown in Figure 17, and the relationship between gas content and TOC content was also referenced. The gas contents of the shales in the Luzhou area were mostly between 11 m^3/t and 17 m^3/t; the shales in the southwestern part of the Luzhou area had higher gas contents (Figure 17). We used the equation below to calculate the amount of gas stored in sub-layer 1 of $Long_1^1$ in the Luzhou area.

$$T = (S \times H \times D \times G)/100$$

where T represents the total gas stored in shales (10^8 m^3); S is the area of Luzhou area in Figure 17 (km^2); H is the shale thickness (m); D is the shale density (t/m^3), with 2.548 t/m^3 used in this calculation; and G is the gas content (m^3/t).

The results show that the gas stored in sub-layer 1 of $Long_1^1$ in the Luzhou area was about 0.62×10^{12} m^3, which is between 0.4×10^{12} m^3 and 1.0×10^{12} m^3, indicating the generated gas calculated according the gas generation model in this study is more accurate. The gas stored in shales being lower than that generated from shales could be attributed to gas migration and loss.

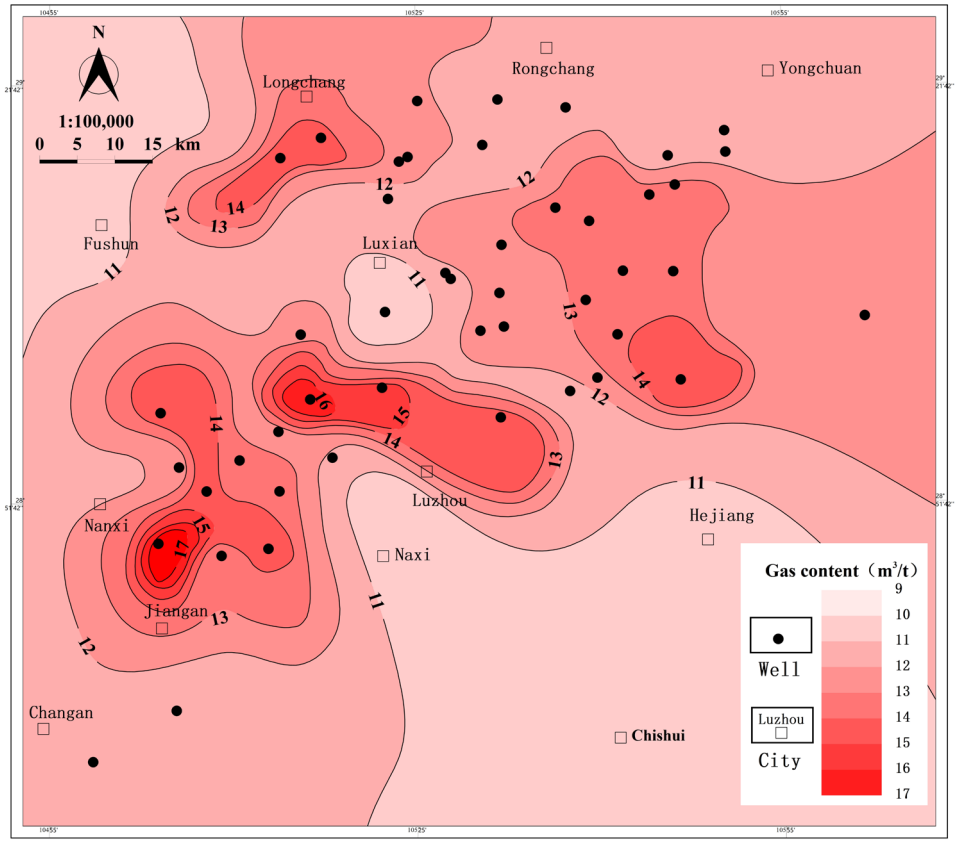

Figure 17. Contour map of gas content from sub-layer 1 of $Long_1^1$ in the Luzhou area.

5. Conclusions

We conducted a series of thermal simulations on a Longmaxi shale sample of relatively low maturity using gold tubes. Then, we established a gas generation model of the Longmaxi shale, and we applied it to sub-layer 1 of $Long_1^1$ in the Luzhou area. Based on these, the following conclusions could be drawn.

(1) The gases generated in our thermal simulations were mainly oil-type gases and kerogen-cracking gases.

(2) The gas generation process of the Longmaxi shale included three stages: (a) the gases were generated quickly in the equivalent vitrinite reflectance ($EqVR_o$) range of 0.5–3.0%; (b) the amount of gas generated was stable in the $EqVR_o$ range of 3.0–3.25%; and (c) the amount of gas generated decreased when $EqVR_o$ exceeded 3.25%.

(3) The calculation results show that the total amount of gas generated in sub-layer 1 of $Long_1^1$ in the Luzhou area was about 1.0×10^{12} m^3, and the gas generation intensities were in the range of 0.4×10^8 m^3/km^2–1.6×10^8 m^3/km^2. In a comparison with the results obtained using other gas generation models, it was found that the accuracy of the gas generation estimation of the Longmaxi shale significantly improved.

Author Contributions: Conceptualization, Y.J.; methodology, Y.J.; software, Z.W.; investigation, Y.F. and Y.G.; resources, X.S., Y.L., Y.Z., W.W. and Z.Z.; writing—original draft preparation, X.S.; writing—review and editing, Y.J.; formal analysis, X.Y.; visualization, X.Y.; supervision, Y.J. and Z.W.; funding acquisition, Y.J. All authors have read and agreed to the published version of the manuscript.

Funding: This research was funded by PetroChina grant number [2023ZZ21YJ04], Shale Gas Research Institute, PetroChina Southwest Oil and Gas Field Company grant number [JS2022-06], and the Natural Science Foundation of Sichuan Province grant number [2024NSFSC0088].

Data Availability Statement: The original contributions presented in this study are included in the article. Further inquiries can be directed to the corresponding authors.

Conflicts of Interest: Xuewen Shi, Yi Li and Wei Wu were employed by Shale Gas Research Institute, PetroChina Southwest Oil & Gasfield Company. The remaining authors declare that the research was con-ducted in the absence of any commercial or financial relationships that could be construed as a potential conflict of interest.

References

1. Tissot, B.P.; Welte, D.H. *Petroleum Occurrence and Formation*; Springer: Berlin, Germany, 1984; p. 699.
2. Zhao, W.Z.; Wang, Z.Y.; Wang, H.J.; Li, Y.X.; Hu, G.Y.; Zhao, C.Y. Further discussion on the connotation and significance of the natural gas relaying generation model from organic materials. *Pet. Explor. Dev.* **2011**, *38*, 129–135. [CrossRef]
3. Hill, R.J.; Zhang, E.; Katz, B.J.; Tang, Y. Modeling of gas generation from the Barnett Shale, Fort Worth Basin, Texas. *AAPG Bull.* **2007**, *91*, 501–521. [CrossRef]
4. Ungerer, P. State of the art of research in kinetic modelling of oil formation and expulsion. *Org. Geochem.* **1990**, *16*, 1–25. [CrossRef]
5. Pepper, A.S.; Corvi, P.J. Simple kinetic models of petroleum formation. Part I: Oil and gas generation from kerogen. *Mar. Petrol. Geol.* **1995**, *12*, 291–319. [CrossRef]
6. Behar, F.; Vandenbroucke, M.; Tang, Y.; Marquis, F.; Espitalie, J. Thermal cracking of kerogen in open and closed systems: Determination of kinetic parameters and stoichiometric coefficients for oil and gas generation. *Org. Geochem.* **1997**, *26*, 321–339. [CrossRef]
7. Lewan, M.D.; Winters, J.C.; McDonald, J.H. Generation of oil-like pyrolyzates from organic-rich shales. *Science* **1979**, *203*, 897–899. [CrossRef] [PubMed]
8. Behar, F.; Kressmann, S.; Rudkiewicz, J.L.; Vandenbroucke, M. Experimental simulation in a confined system and kinetic modeling of kerogen and oil cracking. *Org. Geochem.* **1992**, *19*, 173–189. [CrossRef]
9. Li, Y.; Zhang, J.L.; Xu, Y.H.; Chen, T.; Liu, J.S. Improved understanding of the origin and accumulation of hydrocarbons from multiple source rocks in the Lishui Sag: Insights from statistical methods, gold tube pyrolysis and basin modeling. *Mar. Petrol. Geol.* **2021**, *134*, 105361. [CrossRef]
10. Liu, J.L.; Yang, X.Z.; Liu, K.Y.; Xu, Z.P.; Jia, K.; Zhou, L.; Wei, H.X.; Zhang, L.; Wu, S.J.; Wei, X.Z. Differential hydrocarbon generation and evolution of typical terrestrial gas-prone source rocks: An example from the Kuqa foreland basin, NW China. *Mar. Petrol. Geol.* **2023**, *152*, 106225. [CrossRef]
11. Tannenbaum, E.; Huizinga, B.J.; Kaplan, I.R. Role of minerals in thermal alteration of organic matter. Part II: A material balance. *AAPG Bull.* **1986**, *70*, 1156–1165.
12. Chen, Z.H.; Guo, Q.L.; Jiang, C.Q.; Liu, X.J.; Reyes, J.; Mort, A.; Jia, Z.K. Source rock characteristics and Rock-Eval-based hydrocarbon generation kinetic models of the lacustrine Chang-7 Shale of Triassic Yanchang Formation, Ordos Basin, China. *Int. J. Coal Geol.* **2017**, *182*, 53–65. [CrossRef]
13. Wu, Y.; Zhang, Z.; Sun, L.; Li, Y.; Su, L.; Li, X.; Xu, H.; Tu, Y. The effect of pressure and hydrocarbon expulsion on hydrocarbon generation during pyrolyzing of continental type-III kerogen source rocks. *J. Pet. Sci. Eng.* **2018**, *170*, 958–966. [CrossRef]
14. Gai, H.F.; Tian, H.; Xiao, X.M. Late gas generation potential for different types of shale source rocks: Implications from pyrolysis experiments. *Int. J. Coal Geol.* **2018**, *193*, 16–29. [CrossRef]
15. Lewan, M.D. Experiments on the role of water in petroleum formation. *Geochem. Cosmochim. Acta* **1997**, *61*, 3691–3723. [CrossRef]
16. Burnham, A.K. Comment on "Experiments on the role of water in petroleum formation" by M.D. Lewan. *Geochem. Cosmochim. Acta* **1998**, *62*, 2207–2210.
17. Stainforth, J.G. Practical kinetic modeling of petroleum generation and expulsion. *Mar. Petrol. Geol.* **2009**, *26*, 552–572. [CrossRef]
18. Saxby, J.D.; Riley, K.W. Petroleum generation by laboratory-scale pyrolysis over six years simulating conditions in a subsiding basin. *Nature* **1984**, *308*, 177–179. [CrossRef]
19. Weller, S.; Pelipetz, M.G.; Friedman, S. Kinetics of coal hydrogenation: Conversion of anthraxylon. *Ind. Eng. Chem.* **1951**, *43*, 1575–1579. [CrossRef]
20. Cheng, P.; Xiao, X.M.; Wang, X.; Sun, J.; Wei, Q. Evolution of water content in organic-rich shales with increasing maturity and its controlling factors: Implications from a pyrolysis experiment on a water-saturated shale core sample. *Mar. Petrol. Geol.* **2019**, *109*, 291–303. [CrossRef]
21. Nie, H.K.; Jin, Z.J.; Li, P.; Katz, B.J.; Dang, W.; Liu, Q.Y.; Ding, J.H.; Jiang, S.; Li, D.H. Deep shale gas in the Ordovician-Silurian Wufeng-Longmaxi formations of the Sichuan Basin, SW China: Insights from reservoir characteristics, preservation conditions and development strategies. *J. Asian Earth Sci.* **2023**, *244*, 105521. [CrossRef]

22. Wang, Y.; Qiu, N.; Borjigin, T.; Shen, B.; Xie, X.; Ma, Z.; Lu, C.; Yang, Y.; Yang, L.; Cheng, L.; et al. Integrated assessment of thermal maturity of the Upper Ordovician–Lower Silurian Wufeng–Longmaxi shale in Sichuan Basin, China. *Mar. Petrol. Geol.* **2019**, *100*, 447–465. [CrossRef]
23. Horsfield, B.; Zou, C.N.; Li, J.; Yang, S.Y.; Mahlstedt, N.; Misch, D.; Gross, D.; Ma, W.; Wang, Y.F.; Tan, J.Q. Prediction of the gas-generating characteristics of the Qiongzhusi and Longmaxi Formations, Yangtze Platform, southern China, using analogues. *AAPG Bull.* **2021**, *105*, 945–985. [CrossRef]
24. Luo, Q.Y.; Hao, J.Y.; Skovsted, C.B.; Luo, P.; Khan, I.; Wu, J.; Zhong, N.N. The organic petrology of graptolites and maturity assessment of the Wufeng-Longmaxi Formations from Chongqing, China: Insights from reflectance cross-plot analysis. *Int. J. Coal Geol.* **2017**, *183*, 161–173. [CrossRef]
25. Liu, Y.; Li, C.; Algeo, T.; Fan, J.; Peng, P. Global and regional controls on marine redox changes across the Ordovician-Silurian boundary in South China. *Palaeogeogr. Palaeoclimatol. Palaeoecol.* **2016**, *463*, 180–191. [CrossRef]
26. Zhang, Z.B.; Guo, Y.H.; Zheng, W.Q.; Zeng, C.L.; Li, Y.; Zhao, D.P.; Zhang, J.M. Geochemical characteristics and organic matter enrichment model of Wufeng-Longmaxi formations shale in northeast Sichuan China. *Coal Sci. Technol.* **2024**, *52*, 124–138. (In Chinese with English abstract).
27. Han, H.; He, C.C.; Xiao, S.Q.; Chen, J.T.; Kalmykov, A.; Wu, W.J.; Wang, Y.X.; Wang, J. The Formation of organic matter pores in shales: Implications from combined thermal heating and scanning electron microscopy imaging. *Minerals* **2025**, *15*, 336. [CrossRef]
28. Liu, D.H.; Xiao, X.M.; Tian, H.; Min, Y.S.; Zhou, Q.; Cheng, P.; Shen, J.G. Sample maturation calculated using Raman spectroscopic parameters for solid organics: Methodology and geological applications. *Chin. Sci. Bull.* **2013**, *58*, 1285–1298. [CrossRef]
29. *ISO 7404-2:2009*; Methods for the Petrographic Analysis of Coals-Part 2: Methods of Preparing Coal Samples. International Organization for Standardization: Geneva, Switzerland, 2009.
30. *ASTM D7708-14*; Standard Test Method for Microscopical Determination of the Reflectance of Vitrinite Dispersed in Sedimentary Rocks. ASTM International: West Conshohocken, PA, USA, 2014. Available online: www.astm.org (accessed on 1 May 2014).
31. Sweeney, J.J.; Burnham, A.K. Evaluation of a simple model of vitrinite reflectance based on chemical kinetics. *AAPG Bull.* **1990**, *74*, 1559–1570. [CrossRef]
32. Wang, Z.X.; Wang, Y.L.; Wu, B.X.; Wang, G.; Sun, Z.P.; Xu, L.; Zhu, S.Z.; Sun, L.N.; Wei, Z.F. Hydrocarbon gas generation from pyrolysis of extracts and residues of low maturity solid bitumens from the Sichuan Basin, China. *Org. Geochem.* **2017**, *103*, 51–62. [CrossRef]
33. Jacob, H. Classification, structure, genesis and practical importance of natural solid oil bitumen ("migrabitumen"). *Int. J. Coal Geol.* **1989**, *11*, 65–79. [CrossRef]
34. Dai, J.X. Identification of various alkane gases. *Sci. China Ser. B Chem. Life Sci. Earth Sci.* **1992**, *22*, 185–193, (In Chinese with English abstract).
35. Dai, J.X.; Zou, C.N.; Dong, D.Z.; Ni, Y.Y.; Wu, W.; Gong, D.Y.; Wang, Y.M.; Huang, S.P.; Huang, J.L.; Fang, C.C.; et al. Geochemical characteristics of marine and terrestrial shale gas in China. *Mar. Petrol. Geol.* **2016**, *76*, 444–463. [CrossRef]
36. Li, J.; Li, Z.S.; Wang, X.B.; Wang, D.L.; Xie, Z.Y.; Li, J.; Wang, Y.F.; Han, Z.X.; Ma, C.H.; Wang, Z.H.; et al. New indexes and charts for genesis identification of multiple natural gases. *Petrol. Explor. Dev.* **2017**, *44*, 535–543. [CrossRef]
37. Ma, Z.L.; Shen, B.J.; Pan, A.Y.; Teng, G.; Ning, C.X.; Zheng, L.J. Origin and carbon isotope reversal of shale gas in Wufeng-Longmaxi formations, Sichuan Basin: Implication from pyrolysis experiments. *Petrol. Geol. Exp.* **2020**, *42*, 428–433.
38. Zdanaviciute, O.; Lazauskiene, J. Hydrocarbon migration and entrapment in the Baltic Syneclise. *Org. Geochem.* **2004**, *35*, 517–527. [CrossRef]
39. Dow, W.G. Kerogen studies and geological interpretations. *J. Geochem. Explor.* **1977**, *7*, 79–99. [CrossRef]
40. Waples, D. Time and temperature in petroleum formation: Application of Lopatin's method to petroleum exploration. *AAPG Bull.* **1980**, *64*, 916–926.
41. Xie, Z.Y.; Li, Z.S.; Wei, G.Q.; Li, J.; Wang, D.L.; Wang, Z.H.; Dong, C.Y. Experimental research on the potential of sapropelic kerogen cracking gas and discrimination of oil cracking gas. *Nat. Gas Geosci.* **2016**, *27*, 1057–1066. [CrossRef]
42. Guo, X.S.; Li, Y.P.; Tenger, B.; Wang, Q.; Yuan, T.; Shen, B.J.; Ma, Z.L.; Wei, F.B. Hydrocarbon generation and storage mechanisms of deep-water shales of Ordovician Wufeng Formation-Silurian Longmaxi Formation in Sichuan Basin, China. *Petrol. Explor. Dev.* **2020**, *47*, 193–201. [CrossRef]

Disclaimer/Publisher's Note: The statements, opinions and data contained in all publications are solely those of the individual author(s) and contributor(s) and not of MDPI and/or the editor(s). MDPI and/or the editor(s) disclaim responsibility for any injury to people or property resulting from any ideas, methods, instructions or products referred to in the content.